Imaging sources with fast and slow emission components

G. Verde,[1] D. A. Brown,[2] P. Danielewicz,[1] C. K. Gelbke,[1] W. G. Lynch,[1] and M. B. Tsang[1]
[1]*National Superconducting Cyclotron Laboratory and Department of Physics and Astronomy, Michigan State University, East Lansing, Michigan 48824-1321*
[2]*Lawrence Livermore National Laboratory, Livermore, California 94551-0808*
(Received 3 May 2001; published 2 May 2002)

We investigate two-proton correlation functions for reactions in which fast dynamical and slow evaporative proton emission are both present. In such cases, the width of the correlation peak provides the most reliable information about the source size of the fast dynamical component. The maximum of the correlation function is sensitive to the relative yields from the slow and fast emission components. Numerically inverting the correlation function allows one to accurately disentangle fast dynamical from slow evaporative emission and extract details of the shape of the two-proton source.

DOI: 10.1103/PhysRevC.65.054609 PACS number(s): 25.70.Pq

Intensity interferometry, the investigation of two-particle correlation functions at small relative momenta, can provide important information about the space-time characteristics and underlying dynamics of particle emitting sources [1–6]. At incident energies below the pion threshold, two-proton correlation functions [1,4,5,7–20] have been the tool of choice for studying various equilibrium and nonequilibrium emission processes. Initial analyses of two-proton correlation functions in terms of instantaneous emission from sources with Gaussian density profiles have yielded source radii that strongly depend on the energy of the emitted particles [9,12,13,21], indirectly signaling the importance of lifetime, expansion, and/or cooling effects. Later comparisons of measured correlation functions to predictions of reaction models, assuming either slow evaporative emission [11,12,15] or fast emission according to Boltzmann-Uehling-Uhlenback (BUU) transport calculations [12,13,16–19,21], have provided more quantitative understanding. In particular, some of the correlation functions measured for intermediate-energy nucleus-nucleus collisions have been quantitatively reproduced by BUU transport calculations in a number of cases [12,13,16]. Other data, primarily at higher incident energies [17–19], indicated emission time scales significantly longer than that predicted by BUU transport theory. This led to speculations [19] that proton emission consists of two major components involving significantly different time scales—a fast component consistent with BUU transport theory predictions and a slower component that might originate from the sequential decay of unstable nuclei produced in multifragmentation reactions [19]. Such scenarios may be rather common, with the decay of an equilibrated residue contributing to the slow component at incident energies below the multifragmentation threshold and the decay of excited fragments from multifragmentation processes contributing to the slow component at higher incident energies. When such slow components are present, quantitative comparisons to dynamical models are contingent upon a determination of the relative contributions of these fast and slow components [19].

Up to now, proton-proton correlation function analyses have focused upon obtaining a satisfactory description of the maximum of the correlation function and comparatively little attention was paid to its shape. Numerical inversion techniques have been recently developed [22–24] that provide the capability to analyze the shape of the correlation function and thereby extract much more detailed information about the particle emission mechanism. In this paper, we apply these techniques to analyze correlation functions for systems with strong admixtures of fast and slow emission components. Using general arguments, we show that the width of the correlation peak provides a clear measure of the source size for the fast component and that the height of the correlation peak provides the key information about the relative yields from the fast and slow emission components. We confirm these insights by a detailed reanalysis of the shapes of two-proton correlation functions that were measured previously for $^{14}\mathrm{N}+^{197}\mathrm{Au}$ collisions at $E/A=75$ MeV [12] and were described rather unsatisfactorily [12] by both BUU calculations and by zero-lifetime Gaussian sources.

Experimentally, the (angle-integrated) two-proton correlation function $1+R(q)$ is defined in terms of the two-particle coincidence yield $Y_2(\mathbf{p}_1,\mathbf{p}_2)$ and the single particle yields $Y_1(\mathbf{p}_1)$ and $Y_1(\mathbf{p}_2)$,

$$\sum Y_2(\mathbf{p}_1,\mathbf{p}_2)=C[1+R(q)]\sum Y_1(\mathbf{p}_1)Y_1(\mathbf{p}_2). \quad (1)$$

Here, $\mathbf{p}_1$ and $\mathbf{p}_2$ are the laboratory momenta of the two coincident particles, $q=\mu v_{rel}$ is the momentum of relative motion, and C is a normalization constant chosen such that $\langle R(q)\rangle=0$ for large q where final-state interaction effects are negligible. For a given experimental gating condition, the sums on each side of Eq. (1) extend over all particle energies and detector combinations corresponding to each bin of momentum q.

Theoretical correlation functions are calculated from the angle-averaged Koonin-Pratt formula [1,3,10,23]

$$R(q)=4\pi\int dr(r)^2K(q,r)S(r), \quad (2)$$

where the source function $S(r)$ is defined as the probability distribution for emitting a pair of protons with relative distance r at the time the second proton is emitted. The source function reflects both the spatial extent and lifetime relevant

 ©2002 The American Physical Society

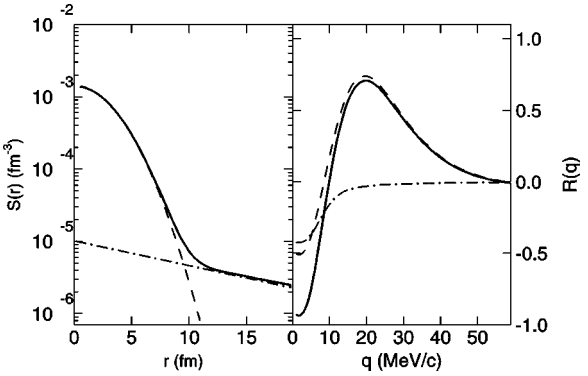

FIG. 1. The solid line indicates a representative two-proton source function for intermediate energy collisions. The dashed and dot-dashed lines provide a decomposition of the solid line into short and long time scale emissions, respectively. Right panel: The solid, dashed and dot-dashed curves show the correlation functions corresponding to the source functions in the left panel.

to single proton emission. An increase in the emission time scale broadens $S(r)$, and for typical proton velocities v_{proton} and time scales τ such that $v_{proton}\tau$ is comparable to or larger than the spatial extent, the complications of finite emission time scales need special consideration [1,5,10,11,14,15,20–25]. The difficult problem posed by the simultaneous presence of very short and very long time scale emissions is discussed below. The angle-averaged kernel $K(q,r)$ is calculated from the radial part of the antisymmetrized two-proton relative wave function. At short distances, $K(q,r)$ is dominated by the strongly attractive singlet *S*-wave proton-proton interaction that gives rise to a maximum in $R(q)$ at relative momentum $q \approx 20$ MeV/c. Both the long-range repulsive Coulomb interaction and antisymmetrization produce a minimum at $q \approx 0$ MeV/c [1]. Both the peaks at $q \approx 20$ MeV/c and the minimum at $q \approx 0$ MeV/c are clearly visible in the correlation function represented by the solid line in the right panel of Fig. 1.

The solid line in the left panel of the same figure represents the source function for this correlation function. Its shape, reflecting both short- and long-ranged components, is representative of intermediate energy heavy ion reactions. The short-ranged contribution, approximated by the dashed line in the left panel, peaks at $r=0$ and originates from fast dynamical emissions that dominate the earlier stages of the reaction. This short-range contribution generates the correlation function described by the dashed line in the right panel. The long-ranged contribution, approximated by long exponential tail at large r values (dot-dashed line, left panel), corresponds to the emission of one or both protons via long time scale secondary decays of excited fragments or the heavy residue, which are produced in the same collision. Unlike the fast component, the secondary decays that contribute to the long-ranged contribution occur over much longer time scales than can be reliably described by the transport theory. Moreover, the influence of this long time-scale component (dot-dashed line, right panel) is negligible everywhere except at $q < 15$ MeV/c, where the Coulomb interaction and the Pauli principle are the major factors and the measurements are very difficult.

The similarity of the dashed and solid lines at $q > 10$ MeV/c in Fig. 1 makes it clear that the correlation function, at such relative momenta, is sensitive only to the fast dynamical portion of this source. However, the long time scale evaporative decays cannot be ignored. To illustrate clearly their influence, let us discuss an extreme example where the emission is dominated by two components, (1) an instantaneous fast component ($\tau_1 = 0$) and (2) a slow component with a sufficiently long decay time scale such that its correlation function is negligible ($\tau_2 \approx \infty$). If fast emission provides a fraction f of the emitted protons, $Y_{1,fast} = fY_1$, and if slow emission provides the remainder, $Y_{1,slow} = (1-f)Y_1$, the resulting correlation function $R(q)$ will reflect only the fast source and will be given by

$$R(q) = f^2 R_{fast}(q) \equiv \lambda R_{fast}(q), \tag{3}$$

where $R_{fast}(q)$ denotes the correlation function when only fast emission is present. Equation (3) stipulates that the height of the correlation function peak, R (20 MeV/c) is attenuated by the factor $\lambda = f^2$; thus, when fast and slow emission processes admix, the height of the correlation peak alone does not determine the source size. However, by its very construction, any property solely derived from the shape of the correlation function for fast emission such as the width of the correlation peak, Δq_{FWHM}, will remain unaffected.

For simplicity, we assume that the fast component has a simple Gaussian profile,

$$S_G(r) = \frac{1}{(2\pi)^{3/2} r_0^3} \exp\left(-\frac{r^2}{2r_0^2} \right), \tag{4}$$

where $\sqrt{3} r_0$ is the Gaussian rms relative proton-proton source radius. For such Gaussian sources, the parameter r_0 describes the spatial distribution of emission points for zero-lifetime sources [1]. For $\lambda = f^2 = 1$, r_0 is uniquely related to the height R (20 MeV/c) (see the curve with $f=1$ in the lower right panel of Fig. 2), and to the width Δq_{FWHM}, (see the top right panel of Fig. 2) of the correlation peak. This simple two-component model (STCM) thus contains two parameters, the Gaussian source radius r_0 and the fraction of coincident pairs resulting from the fast emission components, $\lambda = f^2$. Results obtained with the STCM are illustrated in Fig. 2. Consistent with the previous discussion, the top right panel demonstrates that Δq_{FWHM} depends uniquely on the radius of the fast source, r_0. The bottom right panel demonstrates that R (20 MeV/c) depends on both r_0 and f. The left panel further emphasizes this latter feature by showing that the same value of the correlation maximum can be achieved for different values of r_0 and f.

Thus, measurements of the width Δq_{FWHM} of the correlation function provide a direct measure of the size of the source. Measurements of both Δq_{FWHM} and the correlation function maximum, R (20 MeV/c), provide a unique determination of the relative strengths of equilibrium and dynamical emission components. This finding should remain ap-

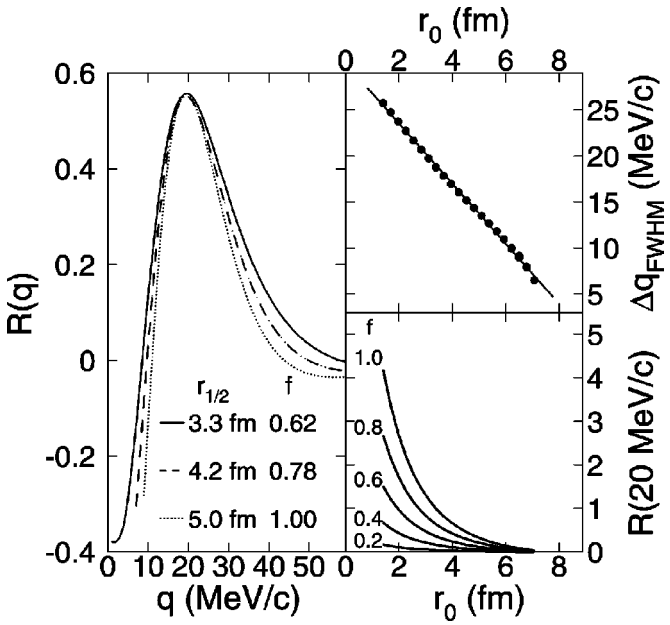

FIG. 2. Two-proton correlation functions predicted with the schematic two-component model (STCM) discussed in the text. The left panel gives examples of correlation functions with similar heights of the correlation peak, but different widths. The top right panel illustrates the unique relation between source size and width of the correlation peak; the line corresponds to a linear best fit to the points. The bottom right panel illustrates the relation between the height of the correlation peak, source radius, and fraction of proton emission originated from fast processes.

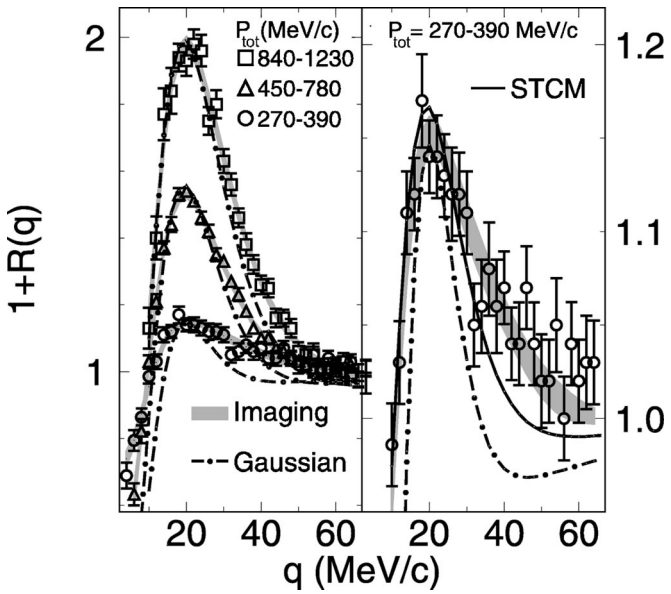

FIG. 3. The left panel shows two-proton correlation functions measured [12] at $\theta_{lab} \approx 25°$ for $^{14}N + ^{197}Au$ collisions at $E/A = 75$ MeV for three different cuts on the total momentum, $P_{tot} = |\mathbf{p}_1 + \mathbf{p}_2|$, of the coincident protons pairs, between 270 MeV/c $< P_{tot} <$ 390 MeV/c (circular points), 450 MeV/$c < P_{tot} <$ 780 MeV/c (triangular points), and between 840 MeV/$c < P_{tot} <$ 1230 MeV/c (square points). The right panel shows the correlation function for the 270 MeV/$c < P_{tot} <$ 390 MeV/c cut on an expanded vertical scale. The various curves are discussed in the text.

proximately valid for more realistic emission time scales, $0 < \tau_{fast} \ll \tau_{slow} < \infty$, provided $v_{proton}\tau_{slow} \gg r_{source}$ and $v_{proton}\tau_{fast} \approx r_{source}$. We emphasize that the correlation function is only sensitive to the details of the long-lived component at very small relative momenta, $q < 15$ MeV/c [1,4,5,11,15], where the long-lived component (dot-dashed line in Fig. 1) generates a nonvanishing correlation function, $R_{slow}(q) \neq 0$. It may be difficult to utilize this sensitivity to probe the details of the long-lived component when the correlation function exhibits a large peak at 20 MeV/c reflecting the additional presence of a strong short-lived component.

We now apply these ideas to the interpretation of two-proton correlation functions measured at $\theta_{lab} \approx 25°$ for $^{14}N + ^{197}Au$ collisions at $E/A = 75$ MeV [12]. The points on the left panel of Fig. 3 show the correlation functions measured for proton pairs with three different cuts on their total momentum $P_{tot} = |\mathbf{p}_1 + \mathbf{p}_2|$, 270 MeV/$c < P_{tot} <$ 390 MeV/c (circular points), 450 MeV/$c < P_{tot} <$ 780 MeV/c (triangular points), and 840 MeV/$c < P_{tot} <$ 1230 MeV/c (square points). As observed for many other reactions [9,12,13,18,19,21], the height of the correlation peak increases with increasing P_{tot}. Correlation functions for zero-lifetime Gaussian sources are shown as dot-dashed curves; the measured values of R (20 MeV/c) can be reproduced by using strongly momentum dependent radius parameters $r_0 = 5.9$ fm, 4.2 fm, and 3.4 fm for the low, medium, and high momentum gates, respectively, but the widths of the correlation function peaks cannot be reproduced by these calculations [12]. Indeed, the widths of the measured correlation functions remain roughly constant at about $\Delta q_{FWHM} \approx 19$–$22$ MeV/c, which implies nearly constant source radii according to Fig. 2. This inconsistency means that these strongly momentum-dependent radius parameters are incorrect.

A somewhat better description of this experimental data can be attained with the STCM by the suitable choice of its free parameters [r_0 and λ in Eqs. (3) and (4)] [26]. The STCM approach describes well data that are dominated by fast dynamical proton emission; the STCM fit for the high momentum gate (840 MeV/$c < P_{tot} <$ 1230 MeV/c) is virtually identical to the fit obtained by the numerical inversion procedure discussed below. (The results of the numerical inversion procedure are shown on the left panel of Fig. 3 by the thick gray curves labeled ''imaging.'') On the other hand, the STCM describes poorly the low momentum data for 270 MeV/$c < P_{tot} <$ 390 MeV/c, which have significant contributions from moderate to very long-lived sources. This is clearly shown in the right panel of Fig. 3, which compares the data, the one-parameter Gaussian analysis (dot-dashed line) and the best-fit STCM analysis (thin solid line) for the low momentum gate. (Note, the vertical scale in the right panel has been magnified to allow more sensitive comparisons; the data, the single Gaussian source-fit, and the numeri-

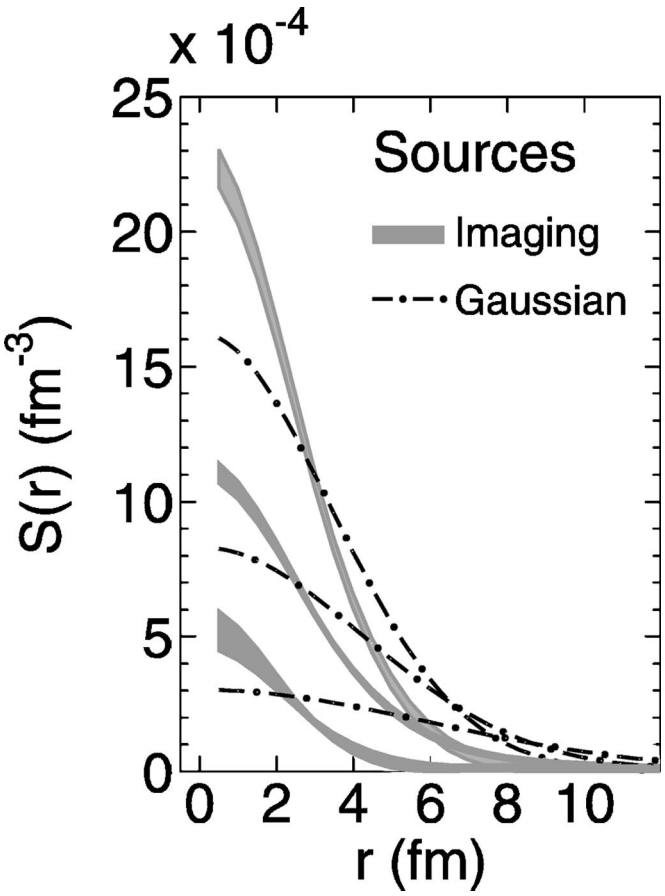

FIG. 4. The grey bands show sources reconstructed from the data (Fig. 3) via the inversion technique of Refs. [22–24]. The dot-dashed lines indicate the sources corresponding to the Gaussian source fits in the left panel of Fig. 3. For both the grey bands and dot-dashed lines, the sources for the highest (lowest) momentum gates have the largest (smallest) values at $r<2$ fm.

cal inversion fit are the same as in the left panel.) Clearly, the best-fit STCM correlation function is wider than the best-fit single Gaussian source correlation function; the STCM source radius of $r_0=4.1$ fm is smaller than the single Gaussian source radius of $r_0=5.9$ fm, consistent with the trends demonstrated in Fig. 2. The measured correlation function is even wider, implying that the true source is smaller than that extracted via the STCM. However, the correct radius information cannot be extracted with the STCM because the shape of the source function is actually not Gaussian. One could attempt to address the mixture of fast and slow components by contructing a model of this mixture [27]. However, we believe that accurate information from correlation functions when there are significant contributions from long-lived sources may be better obtained by avoiding *a priori* assumptions about the shape of the source.

We do this by numerically inverting the correlation functions to construct an image of the emission source as described in Refs. [22–24]. Following Ref. [24], the emission sources $S(r)$ for the protons were parametrized over $0\leqslant r \leqslant 20$ fm by six third-order *b*-spline polynomials, and the numerical inversion of Eq. (2) was achieved via the optimization algorithm of Refs. [23,24]. The thick gray curves in Fig. 3 show the best fits to the experimental data with this imaging approach. The agreement is excellent.

The extracted source functions are shown in Fig. 4. The widths of these curves represent the lower and upper limits defined by σ error bars of the extracted source functions. The uncertainties, small at $r<7$ fm, become very large at $r \geqslant 12$ fm. Better data in the small momentum region ($q<10$ MeV/c) of the correlation functions could provide improved constraints on the source at large radii where the source shape is mainly determined by the time scale of the slow emission component. Unfortunately, this part of the correlation function is difficult to measure and the precision of the data at $q<10$ MeV/c is limited, as shown in the left panel of Fig. 3.

The shapes of the imaged sources and their integrated values at $r\geqslant 12$ fm provide clear evidence for a two-component structure consistent with the occurrence of emission on two very different time scales: a sharply localized central region that can be attributed to a fast emission component, and a tail region that can be attributed to a slow emission component. The half-density radii from the radial source profiles, $r_{1/2}$, and the yield ratio f from the central ($r<3r_{1/2}$) region of the imaged source distributions are given in Table I. Consistent with the weak momentum dependence of the widths Δq_{FWHM} of the measured correlation functions and contrary to the single Gaussian source fits, the source radii vary little with P_{tot}. The strong total momentum dependence of the maximum values of the measured correlation functions reflects the momentum dependence of the relative contributions from the fast dynamical and slow evaporative emitting sources. The fast components dominate

TABLE I. Values for the half radius $r_{1/2}$ and the fraction f of proton emission from the fast component, which have been extracted following the procedures outlined in the text. The label ''Gaussian'' designates the fits using a one-component Gaussian source of Eq. (4). (For the Gaussian profiles, $r_{1/2}\approx 1.18r_0$.)

P_{tot} region	270–390 MeV/c		450–780 MeV/c		840–1230 MeV/c	
	$r_{1/2}$ (fm)	f	$r_{1/2}$ (fm)	f	$r_{1/2}$ (fm)	f
Numerical inversion	2.44 ± 0.37	0.30 ± 0.05	3.13 ± 0.14	0.68 ± 0.03	2.93 ± 0.15	0.78 ± 0.05
Gaussian	7	1	5	1	4	1

the high total momentum gate ($f \approx 0.78$) and become less important at lower momenta where they are reduced to about $f \approx 0.30$ for $P_{tot} = 270–390$ MeV/c. At such low momenta, long-lifetime emissions become more important. This ability of imaging analyses to differentiate between fast and slow emissions will enable more quantitative comparisons with transport theories in the future.

In summary, we have investigated the characteristics of angle-integrated two-proton correlation functions for scenarios in which protons are emitted on two very different time scales. An example of such a scenario would be fast dynamical emission from the initial overlap of projectile and target and slow equilibrium evaporation or secondary decays of particle unstable fragments. When both fast and slow emissions are present, determination of the height and width of the correlation peak allow the extraction of the initial source geometry associated with the fast component and the relative yields from the slow and fast emission processes. More detailed information is obtained by numerically inverting the correlation function. Some additional information about the lifetime of the slow component might be extracted if the detailed shape of the correlation function is measured for very small relative momenta. Precision measurements of angle-integrated two-proton correlation functions may thus provide a valuable diagnostic tool for reactions where fast dynamical and slow equilibrium processes compete. Finally, we note that the simultaneous presence of short and long time scale emissions may also be relevant for two-pion correlations at higher energies where some of the measured particles are produced via the decay of hadronic resonances [6,26–30]. Whether the imaging techniques that are so useful for these analyses of two-proton correlations can be also useful for two-pion correlations is a subject for future investigations.

This work was supported by the National Science Foundation under Grant Nos. PHY-95-28844 and PHY-0070818. Part of this work was performed under the auspices of the U.S. Department of Energy by University of California, Lawrence Livermore National Laboratory under Contract No. W-7405-Eng-48.

[1] S.E. Koonin, Phys. Lett. **70B**, 43 (1977).
[2] M.A. Lisa *et al.*, Phys. Rev. Lett. **84**, 2798 (2000).
[3] S. Pratt and M.B. Tsang, Phys. Rev. C **36**, 2390 (1987).
[4] D.H. Boal, C.K. Gelbke, and B.K. Jennings, Rev. Mod. Phys. **62**, 553 (1990), and references therein.
[5] W. Bauer, C.K. Gelbke, and S. Pratt, Annu. Rev. Nucl. Part. Sci. **42**, 77 (1992), and references therein.
[6] U. Heinz and B.V. Jacak, Annu. Rev. Nucl. Part. Sci. **49**, 529 (1999).
[7] S. Fritz *et al.*, Phys. Lett. B **461**, 315 (1999).
[8] H.A. Gustafsson *et al.*, Phys. Rev. Lett. **53**, 544 (1984).
[9] W.G. Lynch *et al.*, Phys. Rev. Lett. **51**, 1850 (1983).
[10] W.G. Gong *et al.*, Phys. Rev. C **43**, 781 (1991).
[11] W.G. Gong *et al.*, Phys. Lett. B **246**, 21 (1990).
[12] W.G. Gong *et al.*, Phys. Rev. C **43**, 1804 (1991), and references therein.
[13] M.A. Lisa *et al.*, Phys. Rev. Lett. **70**, 3709 (1993).
[14] M.A. Lisa *et al.*, Phys. Rev. Lett. **71**, 2863 (1993).
[15] M.A. Lisa, Phys. Rev. C **49**, 2788 (1994).
[16] D.O. Handzy *et al.*, Phys. Rev. C **50**, 858 (1994).
[17] G.J. Kunde *et al.*, Phys. Rev. Lett. **70**, 2545 (1993).
[18] S.J. Gaff *et al.*, Phys. Rev. C **52**, 2782 (1995).
[19] D.O. Handzy *et al.*, Phys. Rev. Lett. **75**, 2916 (1995).
[20] A. Elmaani *et al.*, Phys. Rev. C **49**, 284 (1994).
[21] F. Zhu *et al.*, Phys. Rev. C **44**, R582 (1991).
[22] D.A. Brown and P. Danielewicz, Phys. Lett. B **398**, 252 (1997).
[23] D.A. Brown and P. Danielewicz, Phys. Rev. C **57**, 2474 (1998).
[24] D.A. Brown and P. Danielewicz, Phys. Rev. C **64**, 014902 (2001).
[25] C.J. Gelderloos *et al.*, Phys. Rev. Lett. **75**, 3082 (1995).
[26] This schematic model recalls the core and halo model introduced to describe two-pion correlation functions [6,27–29] There, the values for λ of less than unity have been interpreted as due to coherent pion emission [31,32] or to the contributions from long-lived resonance decays [6,27–30].
[27] R. Lednicky and M.I. Podgoretskii, Sov. J. Nucl. Phys. **30**, 432 (1979).
[28] R. Lednicky and T.B. Progulova, Z. Phys. C **55**, 295 (1992).
[29] S. Nickerson, T. Csörgő, and D. Kiang, Phys. Rev. C **57**, 3251 (1998).
[30] J.P. Sullivan *et al.*, Phys. Rev. Lett. **70**, 3000 (1993).
[31] M. Biyajima *et al.*, Phys. Rev. C **58**, 2316 (1998).
[32] H. Nakamura *et al.*, Phys. Rev. C **62**, 054903 (2000).